Biochimica et Biophysica Acta 1840 (2014) 1933–1942

Contents lists available at ScienceDirect

Biochimica et Biophysica Acta

journal homepage: www.elsevier.com/locate/bbagen

Persistence length of fascin-cross-linked actin filament bundles in solution and the in vitro motility assay

Hideyo Takatsuki, Elina Bengtsson, Alf Månsson *

Department of Chemistry and Biomedical Sciences, Linnaeus University, Kalmar SE-391 82, Sweden

ARTICLE INFO

Article history:
Received 17 July 2013
Received in revised form 5 January 2014
Accepted 6 January 2014
Available online 10 January 2014

Keywords:
Persistence length
Fascin
Actin
Myosin
Motility assay
Monte-Carlo simulation

ABSTRACT

Background: Bundles of unipolar actin filaments (F-actin), cross-linked via the actin-binding protein fascin, are important in filopodia of motile cells and stereocilia of inner ear sensory cells. However, such bundles are also useful as shuttles in myosin-driven nanotechnological applications. Therefore, and for elucidating aspects of biological function, we investigate if the bundle tendency to follow straight paths (quantified by path persistence length) when propelled by myosin motors is directly determined by material properties quantified by persistence length of thermally fluctuating bundles.

Methods: Fluorescent bundles, labeled with rhodamine-phalloidin, were studied at fascin:actin molar ratios: 0:1 (F-actin), 1:7, 1:4 and 1:2. Persistence lengths (Lp) were obtained by fitting the cosine correlation function (CCF) to a single exponential function: $<\cos(\theta(0) - \theta(s)) > = \exp(-s / (2\mathrm{Lp}))$ where $\theta(s)$ is tangent angle; s: path or contour lengths. $<>$ denotes averaging over filaments.

Results: Bundle-Lp (bundles < 15 μm long) increased from ~10 to 150 μm with increased fascin:actin ratio. The increase was similar for path-Lp (path < 15 μm), with highly linear correlation. For longer bundle paths, the CCF-decay deviated from a single exponential, consistent with superimposition of the random path with a circular path as suggested by theoretical analysis.

Conclusions: Fascin–actin bundles have similar path-Lp and bundle-Lp, both increasing with fascin:actin ratio. Path-Lp is determined by the flexural rigidity of the bundle.

General significance: The findings give general insight into mechanics of cytoskeletal polymers that interact with molecular motors, aid rational development of nanotechnological applications and have implications for structure and in vivo functions of fascin–actin bundles.

1. Introduction

Bundles of actin filaments, cross-linked via the actin-bundling protein fascin, are of key importance in filopodia of motile cells and stereocilia in inner ear sensory cells [1–3]. They have also been tested [4,5] as shuttles [6] for cargo attachment in nanotechnological applications where molecular or nanoscale cargos are transported in vitro [7,8] by surface adsorbed myosin motors or myosin motor fragments such as heavy meromyosin (HMM).

Miniaturization and portability are central in lab-on-a-chip devices [9,10] making it desirable to avoid bulky accessory equipment such as pumps for microfluidics driven separation. One way to achieve this is by the use of ATP-powered molecular motor-driven nanodevices [11,12] where analytes are captured by recognition molecules (e.g. antibodies) immobilized on cytoskeletal filaments [8,13] followed by motor propelled transportation to a detector site [14,15]. Previously both myosin II driven actin filaments [8,16], the motor protein system underlying muscle contraction, and kinesin-1 propelled microtubules [13,17,18], a key cellular cargo-transportation system, have been tested for this purpose. The two systems have different advantages, e.g. higher flexural rigidity of the microtubules and ten-fold faster motility with actomyosin [7,8,12].

The use of fascin–actin bundles as shuttles [4,5] would combine advantageous properties typical of the microtubule-kinesin and actomyosin systems. Thus, like microtubule-kinesin, the bundles have better cargo-carrying capacity than myosin-propelled single actin filaments (F-actin) [4] but they are transported by HMM at similar velocity as the filaments. Furthermore, in similarity to microtubules the bundles have appreciably increased flexural rigidity compared to individual actin filaments associated with increased tendency for the HMM propelled bundles to move in straight paths (corresponding to

Abbreviations: Lp, persistence length; Lp^{M}, persistence length in the motility assay; CCF, cosine correlation function; F-actin, actin filaments; HMM, heavy meromyosin; SDS-PAGE, sodium dodecyl sulfate–polyacrylamide gel electrophoresis; TMCS, trimethylchlorosilane; BSA, bovine serum albumin; ATP, adenosine-5′-triphosphate; MOPS, 4-morpholinepropanesulfonic acid; EGTA, ethylene glycol-bis(2-aminoethylether)-*N*, *N*, *N*′, *N*′-tetraacetic acid; bio-MEMS, bio-microelectromechanical systems

* Corresponding author. Tel.:+46 480 446243; fax: +46 480 446262.
E-mail address: alf.mansson@lnu.se (A. Månsson).

http://dx.doi.org/10.1016/j.bbagen.2014.01.012

higher "path persistence length" [19–21]). This facilitates guiding along micro/nanostructured channels [19] and increases the speed by which cargo may be concentrated, e.g. on a detector site in certain lab-on-chip applications [22]. The dynamic material properties of the bundles, when interacting with myosin motors, may also be important for their roles in e.g. filopodia and stereocilia where such interactions are integral to function.

Whereas the path persistence length is a quantity describing the statistics of the winding path of motor propelled filaments, the persistence length, Lp of a polymer [20,23] characterizes its bending flexibility. Thus, the persistence length of a freely suspended thermally fluctuating polymer is the distance along the polymer over which the "memory" of the tangent angle at a given point is maintained. This persistence length is a material property that is directly proportional to the polymer flexural rigidity EI ($Lp = EI / k_BT$) where E is Young's modulus, I is the second moment of inertia of the polymer cross-section (proportional to the radius raised to the power of 4), k_B is the Boltzmann constant and T is the absolute temperature (cf. [24]). Whereas the path persistence length and the filament persistence length are related quantities [19,20,25] the relationship is not straightforward. Thus, whereas actin filaments without phalloidin stabilization exhibit quantitatively similar path and filament persistence lengths, the path persistence length of phalloidin stabilized actin filaments is almost 50% shorter than the filament persistence length [20]. Even more dramatically, the persistence length of kinesin propelled microtubule paths is only approximately 100 μm [25] compared to a reported filament persistence length of more than 1 mm [26]. This difference has been attributed to a length dependent persistence length of microtubules [27] related to effects of shear forces between microtubule protofilaments [28]. The length dependence would give a low persistence length of the short leading end of the kinesin propelled microtubules whose thermal fluctuations are believed to be the basis of the path persistence length [23,29].

Fascin bundled actin filaments have considerably higher persistence length than actin filaments, an effect that increases with the fascin:actin ratio [30]. However, whereas the HMM-propelled bundle paths are considerably less winding [31] than for HMM propelled actin filaments, the quantitative relationship between the filament and path persistence length is unknown. Insight in this regards is of relevance, in nanotechnological applications, e.g. for understanding the role of cytoskeletal shuttle rigidity in effective cargo transportation and (see above) as a basis for designing nano-, or microstructured surfaces for properly guided bundle transportation. Furthermore, in the in vivo function of fascin–actin bundles, the bundles interact with myosin motors. Finally, the relationship is also of appreciable general interest for mechanistic insight into factors that relate filament persistence length to path persistence length. For instance, in analogy to the situation with microtubules, it seems feasible from theoretical work [29] to expect a lower value of the path persistence length (if this is due to thermal fluctuations of the free leading end of the bundles) than seen for the persistence length of bundles measured in solution Additionally, it is important to consider whether the path persistence length only reflects material properties of the motor propelled polymers [19,20,23,29] or if other factors are important (e.g. [32]). It is also possible that the combination of myosin and fascin binding to actin will lead to propagating changes in material properties as been observed with other combinations of actin-binding proteins [33].

With the aim to address the above issues, we here compare persistence lengths in solution and of HMM propelled paths of F-actin and fascin–actin bundles at fascin:actin ratios with order of magnitude differences in persistence length. The results suggest high degree of linear correlation ($r \approx 1$) between the average persistence length values obtained in these two different ways for bundles and bundle paths shorter than 15–20 μm. However, for paths longer than 20 μm, detailed analysis of the behavior of a large number of HMM propelled bundles demonstrates deviations from a single exponential function of the decay with distance of the cosine correlation function. The results are discussed in relation to nanotechnological applications and the factors determining the relationship between path persistence lengths and the persistence length of the motor propelled filament. Effects of various complicating factors, including bundle heterogeneity, on the shape of the cosine correlation function and numerical persistence length values are discussed. Finally, possible implications for cellular physiology and pathology are considered.

2. Materials and methods

2.1. Protein purifications

Myosin II was isolated from rabbit leg muscles and heavy meromyosin (HMM) was obtained by limited digestion with TLCK-treated α-chymotrypsin [34]. Actin was extracted from acetone powder produced by using leg and back muscles of rabbit [35]. HMM and polymerized actin filaments (F-actin) were frozen in liquid nitrogen in the presence and the absence of 2 mg/ml sucrose, respectively, and stored at −80 °C. F-actin (0.25 mg/ml) was labeled with rhodamine-phalloidin (R415, Invitrogen, USA) at 1:1 actin: rhodamine-phalloidin molar ratio in 10 mM 4-morpholinepropanesulfonic acid (MOPS) buffer at pH 7.0 including 60 mM KCl, 2 mM $MgCl_2$, 0.1 mM ethylene-bis(oxyethylenenitrilo)tetraacetic acid (EGTA) and 3 mM NaN_3. Histidine (His)-tagged fascin was purchased from Novus Biologicals (NBP1-45313, Novus Europe, UK), with a concentration of 0.89 ± 0.29 mg/ml (mean ± 95% confidence interval) according to the Bradford assay. This His-tagged human fascin had been expressed in recombinant *Escherichia coli* and purified in 20 mM Tris–HCl buffer at pH 8.0 including 100 mM NaCl, 2 mM DTT and 20% glycerol as specified by the manufacturer. Fascin–actin bundles were assembled by adding fascin to F-actin (0.25 mg/ml) labeled with rhodamine-phalloidin at different molar ratios (fascin:actin ratios of approximately 1:2, 1:1 and 2:1 (mol:mol)). The protein purity and concentration of proteins (HMM, actin and fascin) were determined by sodium dodecyl sulfate polyacrylamide gel electrophoresis (SDS-PAGE) and protein assays (Bradford or UV absorbance spectroscopy), respectively.

2.2. Actin-bundling assay

Fascin–actin bundles obtained as described above were characterized by a co-sedimentation assay with low-speed centrifugation [36]. Briefly, F-actin (0.25 mg/ml) labeled with rhodamine-phalloidin was mixed gently with human fascin in the desired fascin:actin ratios as described above. After overnight incubation on ice, the actin–fascin mixtures were centrifuged at 12,000 *g* for 40 min. Supernatants and pellets were dissolved in an equivalent amount of Tris–glycine SDS sample buffer (LC2676, Invitrogen) and were run by SDS-PAGE with 12% Bis–Tris gel (NP0342BOX, Invitrogen) in MES SDS running buffer (NP0002, Invitrogen) using molecular-weight markers (LC5925, Invitrogen). Actin and fascin in gels were visualized by a Coomassie Blue staining and quantified by densitometry using ImageJ [37].

2.3. In vitro motility assay

Motility experiments were performed at room temperature (22–23 °C) as described previously [5,38]. For surface modification of glass coverslips with trimethylchlorosilane (TMCS) (92361-100ML, Aldrich, St. Louis, MO), glass cover-slips (60 × 24 mm^2, #0, Menzel-Glaser, Braunschweig, Germany) were first cleaned with piranha solution (H_2SO_4 and 30% H_2O_2 at 7:3 ratio) at 80 °C for 10 min and washed sequentially with H_2O, methanol, acetone and chloroform. The cleaned glass coverslips were then functionalized with 5% TMCS in chloroform for 2 min and washed with chloroform. Flow cells were constructed using double-sided adhesive tape to build a fluid chamber between a non-functionalized small cover-slip (20 × 20 mm^2) and a

TMCS-functionalized large cover-slip (60 × 24 mm^2). For the in vitro motility assays, the flow cells were filled sequentially with the following proteins and chemicals: (1) HMM (120 μg/ml) diluted in buffer A (10 mM MOPS at pH 7.4, 50 mM KCl, 1 mM $MgCl_2$ and 0.1 mM EGTA) for 5 min, (2) bovine serum albumin (BSA, 1 mg/ml) in buffer A for 5 min, (3) buffer B (10 mM MOPS at 7.0, 45 mM KCl and 1 mM $MgCl_2$), (4) F-actin (0.25 μg/ml) or fascin–actin bundles (2.5 μg/ml) labeled with rhodamine-phalloidin in buffer B supplemented with oxygen scavengers (10 mM dithiothreitol, 3 mg/ml glucose, 20 units/ml glucose oxidase and 460 units/ml catalase) and (5) magnesium adenosine-5′-triphosphate (MgATP, 1 mM) in buffer B with oxygen scavengers.

The fluorescent images of F-actin and actin bundles sliding on HMM were captured under an inverted fluorescence microscope (Axio Observer D1, Zeiss, Jena, Germany or Eclipse TE300, Nikon, Tokyo, Japan) using 40×, 63× or 100× objectives (Zeiss: 1.4 N.A. 63× plan-apochromat or 40× plan-neofluar; Nikon: 1.4 N. A. 100× plan-apochromat objective).

The image sequences were recorded using a digital CCD camera (C4742-95, Orca-ER, Hamamatsu Photonics, Hamamatsu, Japan) and the HCImage software (Hamamatsu Photonics) for the Zeiss microscope or an EM-CCD camera (C9100, Hamamatsu Photonics) and SimplePCI software (Hamamatsu Photonics) for the Nikon microscope. The resolution of the recorded images, at an overall image size of 512 × 512 pixels, was 0.32, 0.198 and 0.165 μm/pixel for 40×, 63× and 100× objectives, respectively. The frame rates used were 2 s^{-1} or 4 s^{-1}. The image sequences were analyzed using MatLab software (MatLab R2012b; MathWorks, Natick, MA) to obtain velocity of filament sliding and data for the cosine correlation function (CCF) ($<\cos(\theta(0) - \theta(s))>$), as a basis for subsequent calculation of the persistence length Lp (see below). Image frames for path persistence length analysis were acquired 2–5 min after infusion of ATP-containing assay solution and bundles were selected for analysis on basis of criteria i) that they contained a number of filaments (based on intensity data) that was among the ~50% highest in the image frames studied and ii) that the bundles had apparent low variability in the number of filaments along their length. Most notably, we excluded bundles exhibiting a clearly delineated flexible front end composed of a single or very few filaments. The described semi-quantitative selection approach led to exclusion of the smallest bundles and single filaments formed from disintegration of bundles after ATP addition. This made the population of bundles studied in the in vitro motility assay more similar to the population existing before addition of ATP. Additionally, the selection approach also eliminated the most extreme examples of heterogeneity in bundle composition.

2.4. Thermal fluctuation of filaments and bundles — measurements in solution

Experiments were performed at room temperature (22–23 °C) using a slight modification from the previous study [20,39]. Large glass cover-slips (60 × 24 mm^2) were soaked in a BSA solution at 1 mg/ml for 10 min and then dried with nitrogen gas. BSA-soaked cover-slips were subjected to a droplet (5 μl) of F-actin (0.25 μg/ml) or fascin–actin bundles (2.5 μg/ml) labeled with rhodamine-phalloidin. A small glass cover-slip was placed on this droplet to form a chamber (<5 μm height) between the small and large cover-slips. Subsequently, the chamber was sealed by nail-polish. Thermal fluctuations of F-actin and bundles were visualized using an inverted fluorescence microscope (Zeiss or Nikon; see above) and image sequences were captured using an exposure time of 0.1 s (frame rate 10 s^{-1}). Bundles with thickness approximately in the mid-50% percentile for each fascin:actin ratio were used for the persistence length analysis in solution. In this way we excluded single filaments as well as the largest bundle-like structures, possibly corresponding to loose aggregates of more tightly cross-linked "true" bundles (see further below). Together with the selection procedure for analysis of the path persistence length this also led to an approximate similarity in bundle sizes used for the two sets of analyses.

2.5. Quantitative or semi-quantitative analysis of the number of actin filaments per fascin–actin bundle

In dedicated experiments with results described in detail in the Supplemental Information, we analyzed the variability of filament numbers between bundles and along the length of individual bundles. In these experiments, fluorescence micrographs were obtained at a resolution of 0.165 × 0.165 μm^2/pixel at exposure time of 0.05 s for analysis of the number of filaments per bundle and, generally, 0.5 s for path persistence length measurements. The EMCCD camera gain was adjusted to avoid pixel intensity saturation even for the largest bundles at exposure times of 0.05 s. The average number of filaments per bundle was now obtained, using a MatLab algorithm [8], from the integrated background-subtracted intensity per bundle length divided by the average background-subtracted intensity per length of several single actin filaments. Care was taken to obtain single actin filament and bundle intensities at approximately the same time (within ~5 s) in order to minimize complications due to photo-bleaching.

Representative bundles at different fascin–actin ratios were also selected for semi-quantitative analysis of the filament composition along their length. In this analysis we used ImageJ [37] and images with 0.05 s exposure times to first draw a segmented line along the apparent center of the bundle profile and then obtain a profile pixel intensity plot along this line. With an average sliding velocity between 2 and 4 μm/s, the bundle moved only 0.1–0.2 μm during image acquisition with 0.05 s exposure time, thus negligibly distorting the intensity profile in the in vitro motility assay compared to that of stationary bundles.

2.6. Persistence lengths

Persistence lengths of F-actin and fascin–actin bundles in solution (Lp) and in the motility assay (Lp^M) were obtained by plotting the cosine correlation function (CCF, $<\cos(\theta(s) - \theta(0))>$) against the distance ($s$) along the contour length or the traversed path length of the filaments. In order to obtain s and $\theta(s)$ (defined in Fig. S1), the leading ends of F-actin and fascin–actin bundles were manually tracked using the computer pointer device relying on an algorithm developed in the MatLab environment [20,21]. In the tracking process, velocities of F-actin and bundles were recorded by considering the distance traveled by the filaments and time between measurements. Before the fitting of experimental data (see below) to the CCF, another algorithm was used to identify and exclude filament paths with abrupt direction changes between subsequent frames, e.g., caused by rigor myosin heads [21]. This was done to exclude direction changes unrelated to the normal propulsion due to force-producing actomyosin interactions. The abrupt large direction changes were defined using a cut-off value of 1.5 rad [21].

Persistence lengths in solution (Lp) and the motility assay (Lp^M) were calculated by fitting the CCF to an exponential function:

$$<\cos(\theta(s)-\theta(0))> = \exp\left(-s/\left(2Lp^*\right)\right). \quad (1)$$

Here, $\theta(s)$ represents the tangent angle at a contour length s along the filament (for Lp) or the tangent angle of the sliding direction at distance s along the HMM propelled filament path (for Lp^M) (Fig. S1). Furthermore, Lp^* is substituted in this relationship with either Lp or Lp^M. The symbols "< >" indicate that the difference $\cos(\theta(s) - \theta(0))$ is averaged over a large number of filaments ($N = 74 - 164$). Data were pooled for contour or path length intervals of approximately 1 μm and the mean values of s and the CCF in these intervals were used for the fitting.

In a separate series of experiments, for which details of the results are described in the Supplemental Information, we studied the persistence length at a given fascin–actin ratio as function of the number of filaments per fascin–actin bundle. For this analysis we estimated the number of actin filaments per bundle as described above and then used fits of cosine correlation functions (Eq. (1)) to obtain approximate estimates for the path persistence lengths. This analysis was only semiquantitative due to necessarily limited number of bundles in a certain size-range.

For longer path lengths ($s > 20$ μm) the decay of the cosine correlation function deviated from a single exponential function and was better approximated by the following equation:

$$<\cos(\theta(s)-\theta(0))> = \cos(s/r)\cdot\exp\left(s/\left(2Lp^{M}\right)\right). \quad (2)$$

This equation follows from superimposition of the stochastic winding filament paths upon a deterministic circular path with radius, r (Supplemental Information).

2.7. Monte-Carlo simulations

Sliding paths of actin filaments or fascin–actin bundles were simulated in MatLab, using a Monte-Carlo approach [19,21,40,41] where the sliding direction was updated at defined short time intervals (Δt) with an angular change ($\Delta\theta_{therm}$) from a Gaussian distribution with zero mean value and standard deviation [19]:

$$SD = \sqrt{\frac{v_f \Delta t}{L_P^{theor}}}. \quad (3)$$

Here Lp^{theor} is the theoretical persistence length of the simulated path. The MatLab random number generator for a normal distribution (randn) was used with the standard deviation given by Eq. (3). The product of Δt and the velocity (v_f) correspond to the filament sliding distance between updates in sliding direction. In order to superimpose the stochastic winding filament paths on a deterministic circular path with radius, r, a fixed angular update in sliding direction $\Delta\theta_{fix} = v_f \Delta t/r$ was added to $\Delta\theta_{therm}$.

$$\Delta\theta = \Delta\theta_{therm} + \Delta\theta_{fix}. \quad (4)$$

The simulated filament paths were used as a basis for obtaining the CCF. Persistence lengths were then obtained by fits of Eqs. (1) or (2) as for experimental data.

2.8. Statistical analysis

Data were first analyzed using MatLab software as described above and the subsequent non-linear and linear curve fittings and statistical analyses were performed using Graphpad Prism (version 6.0, Graphpad software, CA). Unless otherwise stated, data are given as mean ± 95% confidence intervals. Comparisons between groups were performed using one-way or two-way analysis of variance (ANOVA) and Tukey's post hoc multiple comparisons test as appropriate.

3. Results and discussion

3.1. Fascin-bundled actin filaments — from assembly to visualization

We assembled actin filaments (F-actin) into uni-polar actin bundles by cross-linking F-actin using His-tagged fascin as schematically indicated in Fig. 1A. A co-sedimentation assay (SDS-PAGE following centrifugation) (Fig. 1B) was used to analyze the purity and composition of F-actin and fascin-mediated actin bundles stabilized with rhodamine-phalloidin. Analyses using SDS-PAGEs were performed on

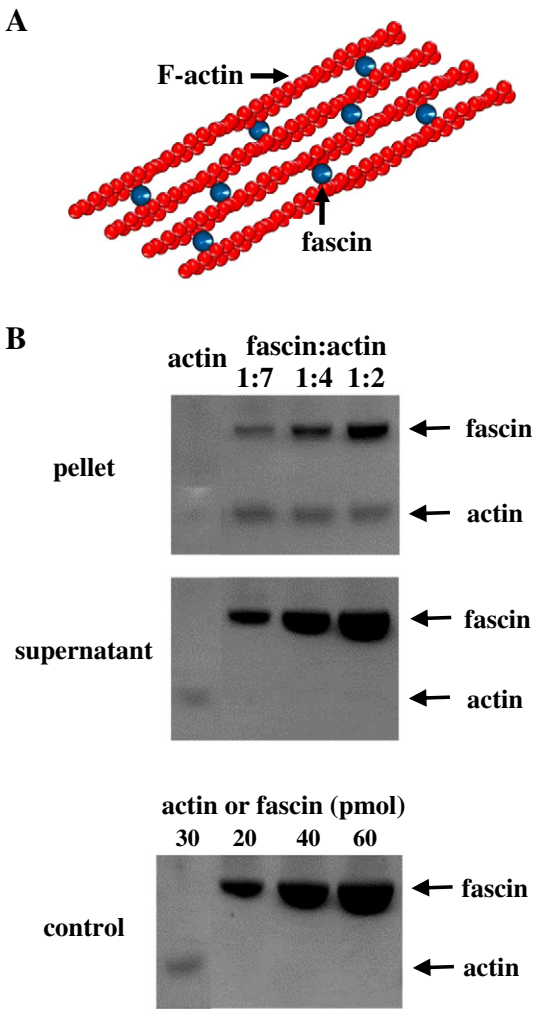

Fig. 1. Structural characteristics of fascin-mediated actin bundle. (A) Schematic diagram of actin bundles showing the bundling of actin filaments (F-actin; red) mediated by fascin (blue). Molecular weights of fascin and actin in monomer form are 57 kDa and 42 kDa, respectively. (B) Actin-bundling assay of rhodamine-phalloidin-stabilized fascin–actin bundles using low-speed centrifugation. Pictures of SDS-PAGE gels visualized by Coomassie staining for the final fascin:actin molar ratios (1:7, 1:4 and 1:2) for pellets (pellet) and supernatant (supernatant) after low-speed centrifugation and for F-actin alone (30 pmol) and fascin alone (20, 40 and 60 pmol) before centrifugation (control).

both pellet and supernatant of fascin–actin mixtures after centrifugation at 12,000 *g*. It can be seen in Fig. 1B (left lanes) that the unbundled F-actin remained to a significant degree in the supernatant whereas the fascin-bundled actin was precipitated in pellet. According to the molecular weights of fascin (57 kDa) and actin (42 kDa) (control in Fig. 1B), fascin–actin bundles in pellets after low-speed centrifugation exhibited the desired positions corresponding to 1:7, 1:4 and 1:2 fascin:actin molar ratios (pellet in Fig. 1B) for 1:2, 1:1 and 2:1 mixing ratios, respectively.

The persistence lengths (Lp) of F-actin and fascin–actin bundles were estimated [20,39] from a large number of fluorescence micrographs (cf. Fig. 2 and Movies S1 and S2) showing snapshots of actin filaments/bundles that execute pseudo-two dimensional thermal motion in solution between two BSA-coated cover-slips. These cover-slips (see Materials and methods section) formed the observation chambers of <5 μm height [20,26,39]. In accordance with earlier results [30], suggesting an order of magnitude higher persistence length of fascin–actin bundles than of F-actin, our fascin–actin bundles showed appreciably less thermal bending fluctuations than F-actin. Moreover they appeared nearly straight or slightly curved on average over the length scales studied (Fig. 2B and Movie S2).

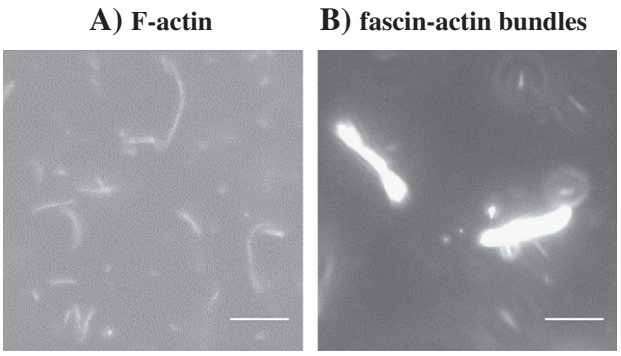

Fig. 2. Fluorescent images of actin filaments (F-actin) (A) and fascin–actin bundles (B; fascin:actin ratio = 1:2) in solution. While F-actin is flexible and curved, fascin–actin bundles are nearly straight and with low flexibility. Scale bars: 10 μm. Details of the image processing are given in the Supplemental Information.

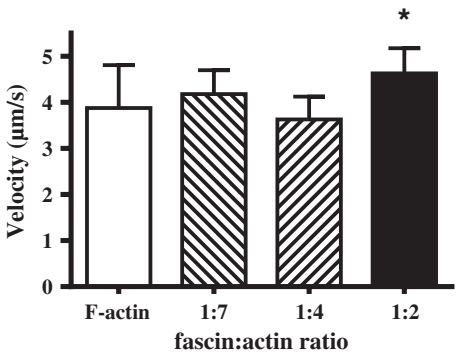

Fig. 4. Mean velocity of sliding actin filaments (F-actin, open bar, $N = 173$ filaments) and fascin–actin bundles propelled by heavy meromyosin (HMM) on the trimethylchlorosilane (TMCS) surface at fascin:actin molar ratios of 1:7 ($N = 73$), 1:4 ($N = 127$) and 1:2 ($N = 164$) in the in vitro motility assay. Data denote mean ± standard deviation from three experiments. * represents a significant difference ($p < 0.0001$) as compared with a mean velocity of F-actin. Room temperature (22–23 °C).

We also estimated the path persistence lengths (Lp^M) [20,25] of both fascin–actin bundles and F-actin when these were propelled by HMM adsorbed to a TMCS-derivatized surface in the presence of 1 mM ATP (Fig. 3). Typical winding trajectories of HMM propelled F-actin (velocity 3.9 ± 0.9 μm/s; mean ± standard deviation, $N = 173$; 21–23 °C) are illustrated in Fig. 3A as well as in Fig. S2A and Movie S3. These winding paths should be contrasted with the nearly straight or slightly curved paths (Fig. 3B, Fig. S2B and Movie S4) often seen for HMM propelled fascin–actin bundles (see also [5,31]). With regard to sliding velocities (Fig. 4), our results are consistent with earlier findings showing no difference between F-actin velocities and the velocities of HMM propelled fascin–actin bundles at the lower fascin–actin ratios (1:7 and 1:4) [4,31]. At higher fascin–actin ratio (1:2) there was a statistically significant increase in velocity compared to F-actin (Fig. 4). This effect might deserve further exploration in future work but this is outside the scope of the present study.

3.2. Bending fluctuations and persistence length measurements

The magnitude of the persistence length of filaments/bundles (Lp) or of HMM propelled filament/bundle paths (Lp^M) was estimated from exponential fits to the CCF, $\langle\cos(\theta(s) - \theta(0))\rangle$, utilizing the relationship (e.g. [42]) in Eq. (1). It can be seen in Fig. 5A that a plot of Lp against s, for F-actin or bundles observed while executing thermal motion in solution, was shifted upwards and to the right for increased fascin:actin ratios, corresponding to increased persistence length. Bundle lengths were consistently less than 15 μm, limiting the range of contour lengths, s, which was possible to study for bundles in solution.

It may be inferred from Fig. 5B that the effects of increased fascin:actin ratio on the CCFs for HMM propelled filament/bundle paths, studied for path lengths shorter than 15 μm, were quantitatively similar

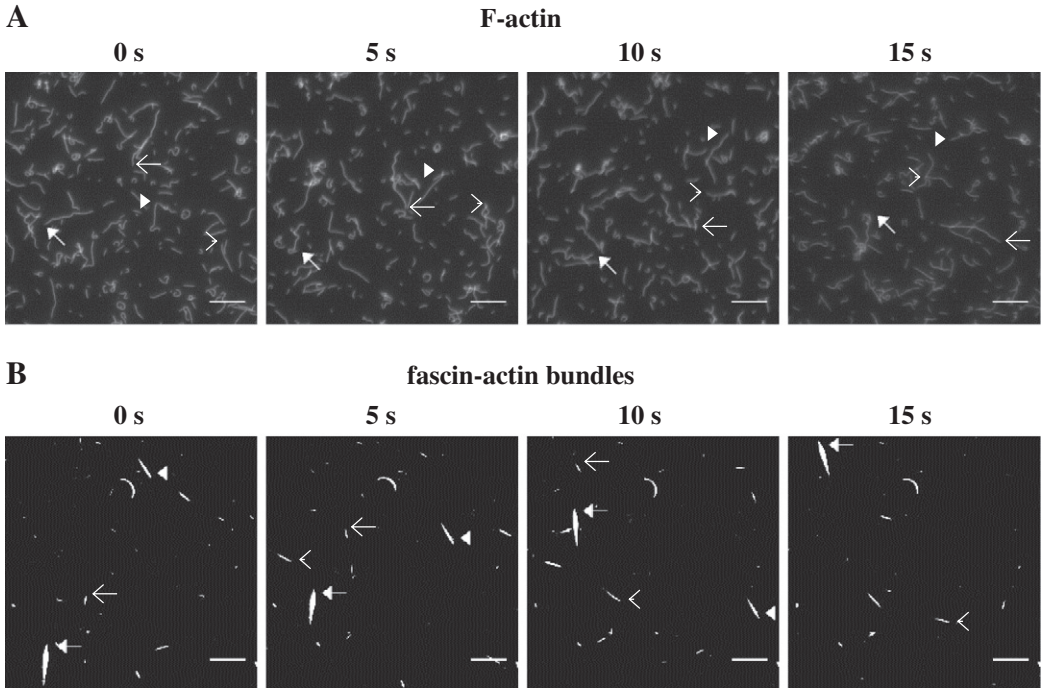

Fig. 3. Image sequences depicting movement of actin filaments (F-actin) (A) and fascin:actin bundles (fascin:actin molar ratio = 1:2) (B) when they are sliding on heavy meromyosin (HMM) for 15 s in the in vitro motility assay. Images represent snapshots (0.5 s exposure time) obtained at 5 s interval. Different arrows denote the tip of individual F-actin and actin bundles during their sliding on HMM. Scale bars: 10 μm. Details of the image processing are given in the Supplemental Information.

to those of filaments/bundles in solution (Fig. 5A). This quantitative agreement is made explicit in Fig. 6 where both the Lp and Lp^M values from the exponential fits in Fig. 5 are plotted against the fascin:actin ratio or against each other (inset Fig. 6, $r \approx 0.98$; slope: 0.94 ± 0.13; mean $\pm$ 95% confidence interval).

As the path lengths of HMM propelled fascin:actin bundles could be tracked as long as the bundles exist in the microscopic field, the CCF could be studied for path lengths up to 80 μm, considerably greater than the readily achievable bundle length (see also [31]). This has the potential to yield insights about bundle properties beyond those that can be obtained by observing thermal motion of the bundles in solution. In this connection it is of interest to note (Fig. 7A) that the CCF was not well described by a single exponential equation in the entire range up to 80 μm, i.e., Eq. (1) is not valid if the entire range is considered. This finding is substantiated by the semi-logarithmic plots in Fig. 7B shown together with fits of Eq. (2) to the data. The deviation from the exponential function suggests that, whereas the path persistence length, measured over a short sliding distance, is fully accounted for by the filament/bundle material properties suggested by observation of bundles in solution (Fig. 6), other factors become of significance at larger sliding distances.

It is relevant to note, in this connection, that deviations from a single exponential function due to worm-like bundle behavior [28], rather than worm-like chain behavior as for a single actin filament, would have different effects than we observed. Under these conditions one would expect reduced, rather than increased, slope of the CCF for large *s*. It is also highly unlikely that the deviation from the exponential function is attributed to statistical fluctuations due to fewer bundles studied for large *s*. This was clear from repeated Monte-Carlo simulations of a limited number of independent bundle paths (Supplementary Information, Fig. S3). First, these simulations suggest that the numbers of bundles studied experimentally (37, 40 and 46 for the 10 μm highest

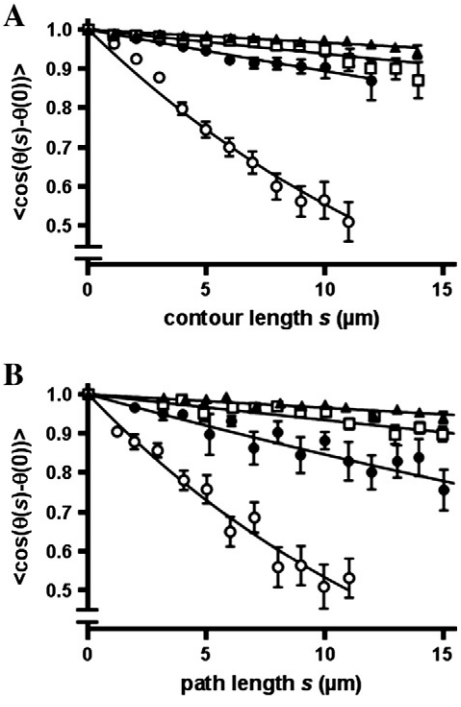

Fig. 5. Cosine correlation functions plotted against contour length *s* along filaments or bundles in solution (A) and against path length *s* from trajectory of filaments or bundles propelled by heavy meromyosin (HMM) on the surface in the in vitro motility assay (B). Experimental data were plotted for actin filaments (F-actin) (open circle) and fascin–actin bundles in the fascin:actin molar ratios of 1:7 (closed circle), 1:4 (open square) and 1:2 (closed triangle). Exponential fits were obtained using non-linear regression.

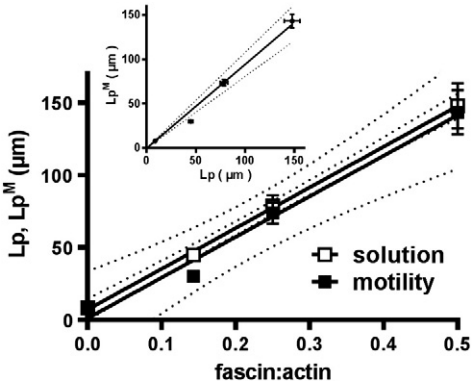

Fig. 6. Effect of fascin and heavy meromyosin (HMM) induced sliding on persistence lengths of actin filaments (F-actin) and fascin–actin bundles. Persistence lengths in the in vitro motility assay (Lp^M; closed squares) and in solution (Lp; open squares) versus the fascin:actin molar ratio. Inset: Lp^M versus Lp for the range of contour lengths and path lengths between $s = 0$ μm to $s = 15$ μm. The quantities Lp and Lp^M were obtained from the exponential fits using the cosine correlation function, as shown in Fig. 5A and B. The straight lines were fitted to the experimental data using linear regression analysis. Lp and Lp^M for actin bundles were considerably larger than for F-actin and increased in proportion to the increased fascin:actin ratios.

s-values at 1:2, 1:4 and 1:7 fascin:actin ratios, respectively) were too high to be compatible with stochastic effects as basis for the observed deviations from an exponential function. Moreover, statistical fluctuations would be expected to go in either direction (Fig. S3) and not consistently downwards, as observed at all fascin:actin ratios studied.

Finally, we also considered the possibility that variability in filament number (see further below) between fascin–actin bundles could underlie the deviation of the CCF from a single exponential. However, Monte-Carlo simulations (not shown) of paths for bundles assumed to have a spectrum of persistence lengths with a uniform distribution (±15%) around an average value, gave CCFs that were similar to those seen if all bundles had a given persistence length equal to the average value.

After rejecting the above hypotheses we instead hypothesized that the increased slope of the CCF of bundles for large path lengths is related to the observation that some fascin–actin bundles followed very well-defined circular paths with radius <100 μm when propelled by HMM (cf. inset of Fig. 7A). Visibly circular paths were excluded from the tracking for the CCF but, it is possible that there was a tendency for circular movement for most bundle paths [43], superimposed on the stochastic motion related to the given persistence length. It is therefore interesting to note that the data in Fig. 7A and B are well fitted by Eq. (2) (see Supplemental Information for derivation). The values of the circle radii, *r*, obtained in this fit were 48 ± 12 μm (mean ± 95% CI), 51 ± 5 μm and 76 ± 7 μm at 1:7, 1:4 and 1:2 fascin:actin ratios. These quantitatively rather similar values are likely to reflect average radii of curvature of the bundle sliding paths. Monte-Carlo simulations in Fig. 7C (developed from method in [40,41]) with random angular changes superimposed on constant amplitude angular changes in sliding direction per update (Eq. (4)) are in accordance with this conclusion.

It is of interest to consider possible mechanisms that could underlie tendencies for circular paths. One obvious possibility is that a large fraction of all bundles have an intrinsic curvature or that a rigid front part of the bundles is bent at a certain angle. Such effects have, to the best of our knowledge, not been explicitly considered previously (e.g. [44,45]). This is however, not surprising as a curvature of high radius may be difficult to unequivocally detect in e.g. electron micrographs. Whereas dedicated electron-microscopy or high-resolution fluorescence microscopy based studies may be required to settle the issue our fluorescence micrographs suggest that at least some bundles are slightly curved (Fig. 2B). Moreover, it is interesting to note that some of the transmission electron micrographs in reference [44] seem to support this view. An alternative possibility to explain a tendency for circular HMM propelled bundle

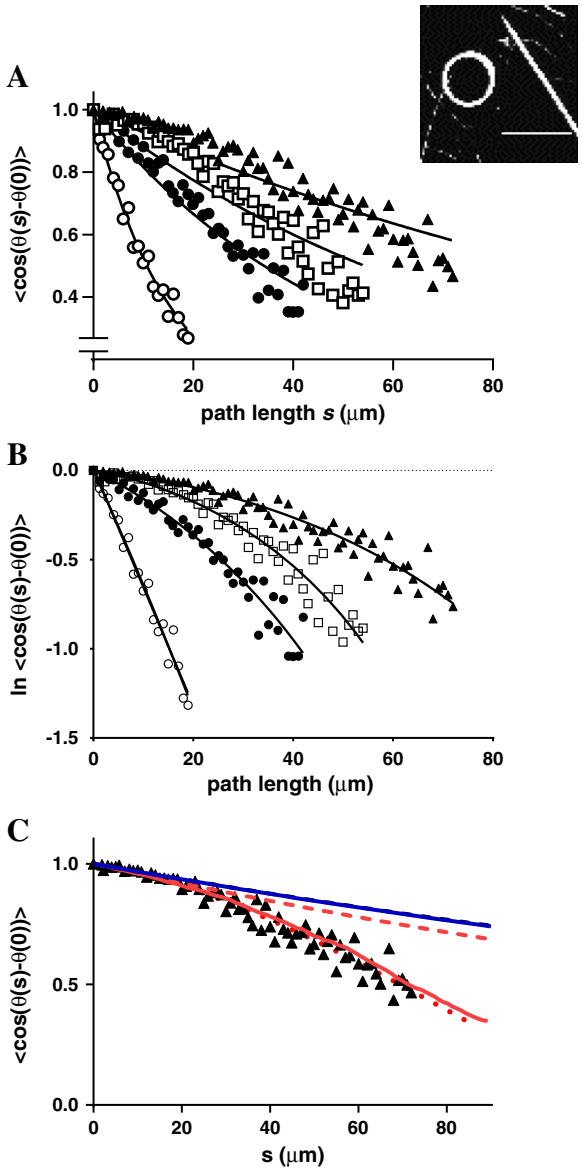

Fig. 7. Cosine correlation functions plotted against path length, *s*, for experimental and simulated data. (A) Experimental data for actin filaments (F-actin) (open circles) and fascin–actin bundles at fascin:actin molar ratios of 1:7 (closed circles), 1:4 (open squares) and 1:2 (closed triangles). Fits of Eq. (1) to experimental data (lines) were obtained using non-linear regression. (Inset) A merged image (total 5 s; all individual images at 0.5 s interval integrated) showing examples of nearly-straight and circular movements of fascin–actin bundles propelled by heavy meromyosin (HMM) (scale bar: 10 μm). (B) Data in A (same meaning of symbols) re-plotted in a semi-logarithmic diagram. Lines represent non-linear regression fits of Eq. (2) to the data followed by logarithmic transformation of the fitted curve. Parameter values obtained in the fitting procedure for different fascin:actin ratios were: 0:1, Lp = 8.2 ± 1.8 μm (*r* not applicable), 1:7, Lp = 36.7 ± 10.3 μm, *r* = 47.7 ± 12.2 μm; 1:4, Lp = 104 ± 37, *r* = 51.2 ± 4.6 μm; 1:2, Lp = 166 ± 54 μm, *r* = 76.5 ± 7.1 μm. (C) Comparison between CCFs based on experimental data for fascin:actin ratio 1:2 (triangles) and simulated data (red full line) assuming sufficient number of simulated paths to suppress statistical fluctuations. It is further assumed in these Monte-Carlo simulations that the filament paths are attributed to random motion, corresponding to a path persistence length of 150 μm superimposed on deterministic circular paths with radii 80 μm (every second clockwise and counter-clockwise, respectively). The dashed lines were obtained by Eq. (1) fitted to the experimental data (black; Lp^M) and the simulated data (red; Lp^M) for s < 20 μm. The dotted red line represents Eq. (2) fitted to all data. The blue line corresponds to the cosine correlation function for simulated filament paths with persistence length of 150 μm without superimposed circular motion.

paths is that the effect results from intrinsic properties of the motor-bundle interactions (cf. [46]). These issues may be elucidated if these interactions are altered e.g. using myosin V or X instead of myosin II or testing different ATP concentrations and motor densities [47,48].

3.3. Number of actin filaments per bundle

The average number of actin filaments (Fig. S4) per HMM propelled fascin–actin bundle with size >1–2 filaments and observed 2–4 min after ATP-addition, was similar for the fascin–actin ratios 1:7 (13.63 ± 2.8; n = 75) and 1:4 (13.21 ± 3; n = 58) but significantly ($p < 0.05$) higher (18 ± 4.1; n = 55) for the 1:2 fascin–actin ratio. These values were significantly lower than those found in the absence of ATP (corresponding to the situation with bundles in solution). Under these conditions we instead observed 25.4 ± 5.3 (n = 55), 34.3 ± 7.6 (n = 64) and 38.0 ± 13.0 (n = 46) filaments per bundle for 1:7, 1:4 and 1:2 fascin–actin ratios. The average bundle sizes in the in vitro motility assay (in the presence of ATP) are similar to those reported previously (14–16 filaments per bundle [31] or ~<20 filaments per bundle [44]) for fascin–actin ratios similar to those used here. In contrast the number of filaments per bundle in the absence of ATP was considerably higher in the present study.

3.4. The path persistence length in relation to the material properties of the bundle/filament

We here show that persistence lengths of the paths and bundles in solution are nearly proportional to each other over a range of more than an order of magnitude provided that the analysis of the CCF is limited to a certain range of filament lengths and path distances (Fig. 6). Moreover, it is important to note that these results relied on selection of the largest bundles to avoid bundles that had been appreciably fragmented by motor action (cf. [31]). Moreover, bundles with a long flexible region in either end were also excluded from the analysis (Fig. S5). This made the bundles in solution and in the motility assay for a given fascin–actin ratio rather similar with respect to the average number of filaments (see further below). One would also expect proportionality between the number of fascin cross-links and the fascin–actin ratio both in solution and in motility assay. In accordance with these assumptions and previous results for Lp [30] we found, in a semi-quantitative analysis (Fig. S6), that Lp^M increased, or tended to increase, both with the number of actin filaments in the bundle and, for a given number of filaments, with the fascin–actin ratio. One somewhat unexpected finding was that the average number of filaments per bundle was significantly higher than 20 in the absence of ATP (Fig. S4) and thus also significantly higher than the upper limitation of the bundle size according to recent findings [44]. One possibility to reconcile these results would be if the largest bundles in our work were actually loose aggregates of more firmly cross-linked bundles of 20 filaments or less. This idea fits nicely with disintegration of most of the largest bundles into bundles with <20 filaments on average upon HMM induced shearing forces in the presence of ATP. The idea would also be consistent with our finding that $Lp = Lp^M$ because the largest bundles that are connected by very weak (few) fascin cross-links would have persistence lengths that are mainly determined by the individual sub-bundles with tightly cross-linked filaments. Moreover, our bundle selection procedures excluded the most extreme bundle sizes from the analysis. Further studies focusing on Lp of the largest bundles will be needed to finally corroborate the idea about loose aggregates. However, due to very limited number of these large bundles such an investigation is outside the scope of the present study.

The results showing significant correlation between path and solution persistence lengths significantly extend previous findings. A direct quantitative agreement between path and filament persistence length has previously been demonstrated [20] only for phalloidin free F-actin over a narrow range of persistence lengths around 10 μm. No similar quantitative correspondence between path and filament persistence length has been demonstrated for microtubules. Although the greater flexural rigidity of microtubule than actin filaments is accompanied by a considerably higher path persistence length (Lp^M) than for HMM propelled actin filaments, Lp for microtubules has been reported to be

more than 1 mm [26], compared to Lp^M of only approximately 100 μm for kinesin propelled microtubule paths. This has been ascribed to a length-dependent persistence length of microtubules with a low persistence length of the filament part (presumed to be the free leading end) that determines the path persistence length [19,27,29]. However, the latter idea has not been unequivocally verified. Therefore, our data set is the first to be fully consistent with the theoretical predictions [23] that the path and polymer persistence lengths are very similar, if not identical. This is interesting as this hypothesis has currently been, at least partly, questioned [32] on basis of the observation of actin–microtubule hybrid polymers propelled either by myosin or kinesin motors.

It has been postulated that thermal fluctuations of the leading end of a motor propelled cytoskeletal filament/bundle determine the path persistence length. However, the leading end of fascin–actin bundles is unlikely to have similar material properties as the bulk of the bundles that would dominate the persistence length measurements from thermal bending fluctuations in solution. First, the bundle end may be without fascin, i.e. the individual filaments may be separated [31] and/or second, the bundle front often has considerably fewer filaments than the bundle bulk and sometimes apparently single filaments may protrude from the front of a bundle (Fig. 8A and B; Movies S5 and S6) with markedly higher flexibility than the bulk. Thus, whereas our results are consistent with the general idea that the persistence length of the motor propelled polymer is similar to that of the path, some of our results suggest that the leading end of the polymer does not necessarily determine the path persistence length. If the leading, usually thinner, end of the bundle (Fig. S7) had determined the path persistence length, the latter would have been expected to be considerably lower than bundle persistence length measured in solution, an average value, dominated by material properties of the central rather rigid part of the bundle (Fig. 8A and B; Fig. S5). In view of the significant correlation between Lp and Lp^M we therefore hypothesized that the flexurally most rigid part of the motor propelled polymer is the major determinant of Lp^M. This part was also dominating in bundles selected for analysis of the persistence lengths in the present work whether in solution or in the in vitro motility assay (Fig. S5). Theoretical support for the view that the flexurally most rigid part of bundle is the major determinant of Lp^M is provided by the analysis in the Supplemental Information. This analysis first suggests that a leading rigid part of a bundle always determines Lp^M, provided that it is not so short that it temporarily detaches from the myosin heads or that rotation around a single attached myosin motor may occur [23]. Also for leading flexible ends shorter than 1 μm the Supplemental Analysis shows that a rigid trailing end fully determines the path persistence length. Because a vast majority of the HMM propelled bundles had a leading rigid end or a leading flexible end shorter than 1 μm (Fig. S5) and because bundles with longer flexible front ends were not selected for analysis it seems clear that the most flexurally rigid bundle parts generally determine Lp^M. Indeed, the analysis in the Supplemental Theory suggests that even with a leading flexible end appreciably longer than 1 μm, the trailing rigid end has major influence on Lp^M. This effect is illustrated in the experiment in Fig. 8 showing a HMM propelled fascin–actin bundle having a single filament at the front. The latter filament frequently changed its tangent angle considerably more than the bulk of the bundle but the HMM propulsion of this bulk had major influence over the sliding direction.

The analysis in the Supplemental Theory (cf. Eqs. S2, S6–S8) also seems to lend support to the idea [32] that the degree of processivity of the motor protein may have some influence on the path persistence length. Nevertheless, the strong correlation of the numerical values of Lp and Lp^M shows that the material properties of the motor propelled polymer constitute a major determinant of the path persistence length.

One may argue that this model is inconsistent with observations [32] that myosin propelled actin filaments, cross-linked to microtubules, exhibited a path persistence length similar to that of myosin propelled actin filaments alone. However, the more rigid microtubules would prevent elastic equilibration of actin filaments only if the link between the two types of cytoskeletal filaments was at least as stiff as the microtubules (see further [28]). This was most likely not the case as the linking was achieved using rather sparse streptavidin–biotin links.

Another possible complication would be if not only the number of fascin cross-links and the number of actin filaments per bundle increases with the fascin–actin ratio but also the number of actomyosin interactions. However, the latter number would, a priori, be expected to scale with an exponent of 0.5 with the number of actin filaments and fascin cross-links. This follows from the fact that the actin filaments that may interact with myosin heads are only those on the surface of the bundle. Indeed, there is evidence [5,31] from analysis of the myosin surface density that is required to hold and propel the bundles at maximum velocity on the surface that the scaling exponent is instead close to 0, i.e. the number of actin–myosin interactions does not increase

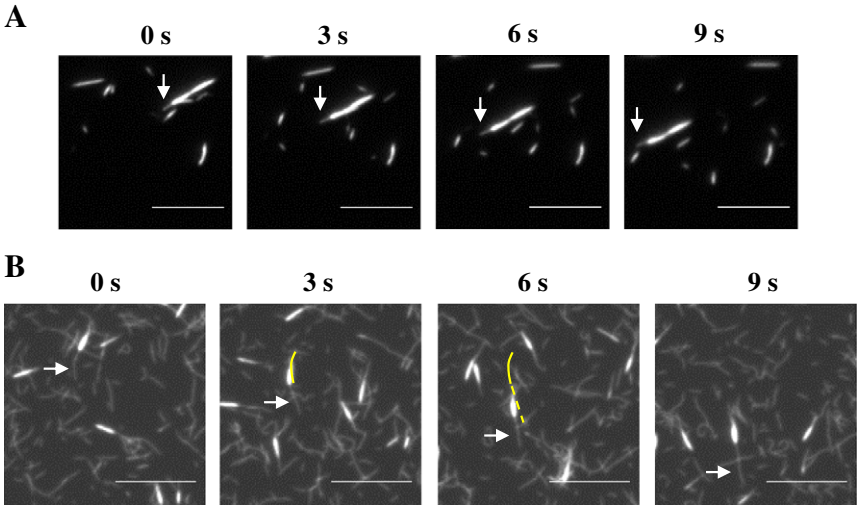

Fig. 8. Image series showing HMM-driven movement of fascin–actin bundles, each having short, apparently individual, actin filament at the front end as indicated by arrows. Actin filaments at the front end of bundles are shorter (A) and longer (B) than the thick part of bundles. In (B) the position of the single filament at the leading end at time 0 s is illustrated by yellow full lines in the figures at times 3 s and 6 s. The position of single filament at front at time 3 s is illustrated by dashed yellow line in figure at time 6 s. Scale bar: 10 μm. Details of the image processing are given in the Supplemental Information.

with bundle size. Therefore, appreciably altered number of actomyosin interactions with altered bundle size is unlikely to have major influence of the path persistence length. It also seems highly unlikely that such influence should balance those of other complicating factors to give a nearly perfect correlation between L_P and Lp^M with slope close to 1. It seems more likely that L_P and Lp^M reflect the same properties, i.e. the material properties of the fascin–actin bundles. Furthermore, related to this observation, our results suggest that myosin binding has negligible effects on the persistence length of fascin–actin bundles in contrast to previous results with phalloidin-labeled F-actin [20,49].

3.5. Nanotechnological applications

In molecular shuttle systems, cytoskeletal filaments (actin filaments and microtubules) move on molecular motors (myosin and kinesin, respectively) to carry nano- and micro-sized cargos on engineered surfaces, e.g. to a detection site [12,50]. To guide filament movement to a certain location on a chip, nano- or micro-channels are required [5,38,51,52]. Especially the need for narrower channel [19] is essential for the lower persistence length of the filament path. Furthermore, increased persistence length will also be advantageous for rapid transportation to a detector site in some geometries [22]. In this regard, the >10 times lower Lp^M of F-actin–myosin, compared to microtubule–kinesin, is a disadvantage [20,25]. In contrast, our experiments with fascin–actin bundles demonstrate that Lp^M of bundles is comparable to that of kinesin propelled microtubules ($Lp^M = \sim 140$ μm for bundles at 1:2 fascin:actin ratio (Fig. 6); vs. $Lp^M = \sim 100$ μm for microtubules [25]). Thus, fascin–actin bundles improve the directional control of HMM-propelled transport while maintaining the high velocity of HMM-propelled F-actin (Fig. 4), i.e., up to 10 times higher than that of microtubule movement propelled by kinesin [4,12]. This is of appreciable interest, considering that fascin–actin bundles enable HMM-driven transport of large-sized cargos (e.g. *E. coli* cells) [4] and our results suggest that the most optimized design will be achieved using high fascin:actin ratio.

3.6. Biological relevance

In biological systems, the assembly and disassembly of F-actin and actin bundles as well as actomyosin interactions occur frequently in dynamic actin networks during cell growth and motility [3]. In relation to actin bundles induced by fascin, filopodia at growth cones in nerve cells and other motile cells play an important role in the search for the localized environment of guidance cues which control the direction of axon toward desired locations [53–55]. Fascin-induced actin-bundle formation is related to filopodial turning, elongation and retraction. Our results demonstrate that flexural rigidity of actin filaments and bundles is little reduced by myosin binding unlike shown in some cases [20,49,56] for F-actin (Fig. 6). The high flexural rigidity is supportive of mechanical and morphological properties of myosin-propelled actin bundles to influence filopodial elongation and changes in direction [57]. Fascin-induced actin bundles regulate the deformation of filopodia under mechanical stress and myosin motor activity (demonstrated with myosin V) [58] may cause autonomous rotations of filopodia, possibly related to the HMM induced circular movements observed here (Fig. 7).

Actin-bundling proteins are not only involved in maintenance of the physiological functions and structures in normal cells. They are also of relevance in pathological processes, e.g. in tumor cells [2,59]. Although human fascin is expressed normally in cells derived from mesenchymal and epithelial tissues, over-expression of fascin is induced in many types of cancers where it facilitates the invasive potentials of tumor cells [60]. The increased flexural rigidity at increased fascin:actin ratio that we observe here is higher than seen under in vivo physiological conditions (Figs. 4 and 6). The increased mechanical rigidity of fascin–actin bundles with or without motor actions may be an essential factor in the invasive and metastatic potentials of cancer cells, e.g. in their capability to spread through a dense environment. This suggests that fascin expression and the fascin–actin interactions are interesting targets for drug therapy.

4. Conclusions

We demonstrate that fascin-bundled actin filaments exhibit considerably higher persistence length (higher flexural rigidity) than single actin filaments (F-actin) and that the persistence length increases in direct proportion to the increased fascin:actin ratio. Furthermore, these effects are not influenced by myosin motor action as our results show good agreement between persistence lengths of bundles measured from thermal bending fluctuations in solution and path persistence lengths obtained in motility assays with HMM propelled bundles. Indeed, this is the first unequivocal corroboration of the hypothesis [23] that the two persistence length values should be identical and that the path persistence length therefore provides direct information about the material properties of myosin-propelled polymers. In a different perspective, it is clarified that the fascin:actin ratios can control the bending stiffness of fascin–actin bundles during the sliding on HMM and this is of relevance for the optimized use of actin–myosin-based transport systems in nanotechnological application, e.g., biosensors, lab-on-a-chip systems and bio-micromechanical systems (bio-MEMS). Finally, our results should be considered in relation to the dynamic structural and mechanical properties of filopodia in health and disease (e.g. tumor progression and metastasis).

Supplementary data to this article can be found online at http://dx.doi.org/10.1016/j.bbagen.2014.01.012.

Conflict of interest

AM is a co-founder, co-owner and CEO of the start-up company ActoSense Biotech AB (Kalmar, Sweden) aiming to develop diagnostic devices based on the aggregation of cytoskeletal elements, particularly actin filaments, in solution. Moreover, AM holds two Swedish patents in this field and one US patent (about aggregation of actin filaments by analyte molecules) was recently approved. Additional related patent applications have been filed in Sweden and throughout Europe.

Acknowledgement

This work was funded by The Carl Trygger Foundation, The Crafoord Foundation, The Swedish Research Council (Project # 621-2010-5146) and the Faculty of Natural Sciences and Engineering and the Faculty of Health and Life Sciences at the Linnaeus University. We thank Prof. Kazuhiro Kohama, Gunma University in Japan and our lab colleagues, Linnaeus University for helping with the initial experiments and discussions.

References

[1] R.A. Edwards, J. Bryan, Fascins, a family of actin bundling proteins, Cell Motil. Cytoskeleton 32 (1995) 1–9.
[2] L. Chen, S. Yang, J. Jakoncic, J.J. Zhang, X.Y. Huang, Migrastatin analogues target fascin to block tumour metastasis, Nature 464 (2010) 1062–1066.
[3] D.A. Fletcher, R.D. Mullins, Cell mechanics and the cytoskeleton, Nature 463 (2010) 485–492.
[4] H. Takatsuki, H. Tanaka, K.M. Rice, M.B. Kolli, S.K. Nalabotu, K. Kohama, P. Famouri, E.R. Blough, Transport of single cells using an actin bundle–myosin bionanomotor transport system, Nanotechnology 22 (2011) 245101.
[5] H. Takatsuki, K.M. Rice, S. Asano, B.S. Day, M. Hino, K. Oiwa, R. Ishikawa, Y. Hiratsuka, T.Q. Uyeda, K. Kohama, E.R. Blough, Utilization of myosin and actin bundles for the transport of molecular cargo, Small 6 (2010) 452–457.
[6] H. Hess, J. Clemmens, D. Qin, J. Howard, V. Vogel, Light-controlled molecular shuttles made from motor proteins carrying cargo on engineered surfaces, Nano Lett. 1 (2001) 235–239.
[7] M. Lard, L. TenSiethoff, M. Persson, A. Kumar, H. Linke, A. Månsson, Ultrafast molecular motor driven nanoseparation and biosensing, Biosens. Bioelectron. 48 (2013) 145–152.

[8] S. Kumar, L. ten Siethoff, M. Persson, M. Lard, G. te Kronnie, H. Linke, A. Månsson, Antibodies covalently immobilized on actin filaments for fast myosin driven analyte transport, PLoS ONE 7 (2012) e46298.
[9] D.A. Giljohann, C.A. Mirkin, Drivers of biodiagnostic development, Nature 462 (2009) 461–464.
[10] G.M. Whitesides, The origins and the future of microfluidics, Nature 442 (2006) 368–373.
[11] A. Agarwal, H. Hess, Biomolecular motors at the intersection of nanotechnology and polymer science, Prog. Polym. Sci. 35 (2010) 252–277.
[12] T. Korten, A. Mansson, S. Diez, Towards the application of cytoskeletal motor proteins in molecular detection and diagnostic devices, Curr. Opin. Biotechnol. 21 (2010) 477–488.
[13] S. Ramachandran, K.H. Ernst, G.D. Bachand, V. Vogel, H. Hess, Selective loading of kinesin-powered molecular shuttles with protein cargo and its application to biosensing, Small 2 (2006) 330–334.
[14] C.T. Lin, M.T. Kao, K. Kurabayashi, E. Meyhofer, Self-contained, biomolecular motor-driven protein sorting and concentrating in an ultrasensitive microfluidic chip, Nano Lett. 8 (2008) 1041–1046.
[15] T. Fischer, A. Agarwal, H. Hess, A smart dust biosensor powered by kinesin motors, Nat. Nanotechnol. 4 (2009) 162–166.
[16] A. Mansson, M. Sundberg, M. Balaz, R. Bunk, I.A. Nicholls, P. Omling, S. Tagerud, L. Montelius, In vitro sliding of actin filaments labelled with single quantum dots, Biochem. Biophys. Res. Commun. 314 (2004) 529–534.
[17] A. Carroll-Portillo, M. Bachand, G.D. Bachand, Directed attachment of antibodies to kinesin-powered molecular shuttles, Biotechnol. Bioeng. 104 (2009) 1182–1188.
[18] C.M. Soto, B.D. Martin, K.E. Sapsford, A.S. Blum, B.R. Ratna, Toward single molecule detection of staphylococcal enterotoxin B: mobile sandwich immunoassay on gliding microtubules, Anal. Chem. 80 (2008) 5433–5440.
[19] T. Nitta, A. Tanahashi, Y. Obara, M. Hirano, M. Razumova, M. Regnier, H. Hess, Comparing guiding track requirements for myosin- and kinesin-powered molecular shuttles, Nano Lett. 8 (2008) 2305–2309.
[20] P.G. Vikhorev, N.N. Vikhoreva, A. Mansson, Bending flexibility of actin filaments during motor-induced sliding, Biophys. J. 95 (2008) 5809–5819.
[21] E. Bengtsson, M. Persson, A. Mansson, Analysis of flexural rigidity of actin filaments propelled by surface adsorbed myosin motors, Cytoskeleton (Hoboken) 70 (2013) 718–728.
[22] T. Nitta, H. Hess, Effect of path persistence length of molecular shuttles on two-stage analyte capture in biosensors, Cell. Mol. Bioeng. 6 (2012) 109–115.
[23] T. Duke, T.E. Holy, S. Leibler, Gliding assays for motor proteins — a theoretical-analysis, Phys. Rev. Lett. 74 (1995) 330–333.
[24] J. Howard, Mechanics of Motor Proteins and the Cytoskeleton, Sinauer Associates Inc., Sunderland, MA, 2001.
[25] T. Nitta, H. Hess, Dispersion in active transport by kinesin-powered molecular shuttles, Nano Lett. 5 (2005) 1337–1342.
[26] F. Gittes, B. Mickey, J. Nettleton, J. Howard, Flexural rigidity of microtubules and actin-filaments measured from thermal fluctuations in shape, J. Cell Biol. 120 (1993) 923–934.
[27] F. Pampaloni, G. Lattanzi, A. Jonas, T. Surrey, E. Frey, E.L. Florin, Thermal fluctuations of grafted microtubules provide evidence of a length-dependent persistence length, Proc. Natl. Acad. Sci. U. S. A. 103 (2006) 10248–10253.
[28] C. Heussinger, F. Schuller, E. Frey, Statics and dynamics of the wormlike bundle model, Phys. Rev. E Stat. Nonlinear Soft Matter Phys. 81 (2010) 021904.
[29] M.G. Van den Heuvel, M.P. de Graaff, C. Dekker, Microtubule curvatures under perpendicular electric forces reveal a low persistence length, Proc. Natl. Acad. Sci. U. S. A. 105 (2008) 7941–7946.
[30] M.M. Claessens, M. Bathe, E. Frey, A.R. Bausch, Actin-binding proteins sensitively mediate F-actin bundle stiffness, Nat. Mater. 5 (2006) 748–753.
[31] R. Ishikawa, T. Sakamoto, T. Ando, S. Higashi-Fujime, K. Kohama, Polarized actin bundles formed by human fascin-1: their sliding and disassembly on myosin II and myosin V in vitro, J. Neurochem. 87 (2003) 676–685.
[32] D.S. Choi, K.E. Byun, S. Hong, Dual transport systems based on hybrid nanostructures of microtubules and actin filaments, Small 7 (2011) 1755–1760.
[33] Z. Ujfalusi, M. Kovacs, N.T. Nagy, S. Barko, G. Hild, A. Lukacs, M. Nyitrai, B. Bugyi, Myosin and tropomyosin stabilize the conformation of formin-nucleated actin filaments, J. Biol. Chem. 287 (2012) 31894–31904.
[34] S.J. Kron, Y.Y. Toyoshima, T.Q. Uyeda, J.A. Spudich, Assays for actin sliding movement over myosin-coated surfaces, Methods Enzymol. 196 (1991) 399–416.
[35] J.D. Pardee, J.A. Spudich, Purification of muscle actin, Methods Cell Biol. 24 (1982) 271–289.
[36] S. Yamashiro-Matsumura, F. Matsumura, Purification and characterization of an F-actin-bundling 55-kilodalton protein from HeLa cells, J. Biol. Chem. 260 (1985) 5087–5097.
[37] C.A. Schneider, W.S. Rasband, K.W. Eliceiri, NIH image to ImageJ: 25 years of image analysis, Nat. Methods 9 (2012) 671–675.
[38] M. Sundberg, J.P. Rosengren, R. Bunk, J. Lindahl, I.A. Nicholls, S. Tagerud, P. Omling, L. Montelius, A. Mansson, Silanized surfaces for in vitro studies of actomyosin function and nanotechnology applications, Anal. Biochem. 323 (2003) 127–138.
[39] A. Ott, M. Magnasco, A. Simon, A. Libchaber, Measurement of the persistence length of polymerized actin using fluorescence microscopy, Phys. Rev. E Stat. Phys. Plasmas Fluids Relat. Interdiscip. Top. 48 (1993) R1642–R1645.
[40] T. Nitta, A. Tanahashi, M. Hirano, H. Hess, Simulating molecular shuttle movements: towards computer-aided design of nanoscale transport systems, Lab Chip 6 (2006) 881–885.
[41] A. Månsson, R. Bunk, M. Sundberg, L. Montelius, Self-organization of motor propelled cytoskeletal filaments at topographically defined borders, J. Biomed. Biotechnol. 2012 (2012) 647265.
[42] L.D. Landau, E.M. Lifshitz, Statistical Physics, Pergamon Press, Oxford, 1980.
[43] V. Schaller, C.A. Weber, B. Hammerich, E. Frey, A.R. Bausch, Frozen steady states in active systems, Proc. Natl. Acad. Sci. U. S. A. 108 (2011) 19183–19188.
[44] M.M. Claessens, C. Semmrich, L. Ramos, A.R. Bausch, Helical twist controls the thickness of F-actin bundles, Proc. Natl. Acad. Sci. U. S. A. 105 (2008) 8819–8822.
[45] H. Murakami, T. Ishikawa, M. Sano, The relaxing effect of SKF 38393 on the catch contraction of *Mytilus* smooth muscle, Gen. Pharmacol. 17 (1986) 685–687.
[46] S. Pyrpassopoulos, E.A. Feeser, J.N. Mazerik, M.J. Tyska, E.M. Ostap, Membrane-bound myo1c powers asymmetric motility of actin filaments, Curr. Biol. CB 22 (2012) 1688–1692.
[47] B.L. Ricca, R.S. Rock, The stepping pattern of myosin X is adapted for processive motility on bundled actin, Biophys. J. 99 (2010) 1818–1826.
[48] A. Vilfan, Twirling motion of actin filaments in gliding assays with nonprocessive myosin motors, Biophys. J. 97 (2009) 1130–1137.
[49] T. Yanagida, M. Nakase, K. Nishiyama, F. Oosawa, Direct observation of motion of single F-actin filaments in the presence of myosin, Nature 307 (1984) 58–60.
[50] A. Mansson, Translational actomyosin research: fundamental insights and applications hand in hand, J. Muscle Res. Cell Motil. 33 (2012) 219–233.
[51] M. Sundberg, R. Bunk, N. Albet-Torres, A. Kvennefors, F. Persson, L. Montelius, I.A. Nicholls, S. Ghatnekar-Nilsson, P. Omling, S. Tagerud, A. Mansson, Actin filament guidance on a chip: toward high-throughput assays and lab-on-a-chip applications, Langmuir 22 (2006) 7286–7295.
[52] M.B. Kolli, B.S. Day, H. Takatsuki, S.K. Nalabotu, K.M. Rice, K. Kohama, M.K. Gadde, S.K. Kakarla, A. Katta, E.R. Blough, Application of poly(amidoamine) dendrimers for use in bionanomotor systems, Langmuir 26 (2010) 6079–6082.
[53] H. Takatsuki, A. Sakanishi, Regulation of neurite outgrowth by extracellular Ca^{2+} for neural cells PC12 and PC12D, Colloids Surf. B 32 (2003) 69–76.
[54] Y.S. Aratyn, T.E. Schaus, E.W. Taylor, G.G. Borisy, Intrinsic dynamic behavior of fascin in filopodia, Mol. Biol. Cell 18 (2007) 3928–3940.
[55] Y. Sasaki, K. Hayashi, T. Shirao, R. Ishikawa, K. Kohama, Inhibition by drebrin of the actin-bundling activity of brain fascin, a protein localized in filopodia of growth cones, J. Neurochem. 66 (1996) 980–988.
[56] A. Orlova, E.H. Egelman, A conformational change in the actin subunit can change the flexibility of the actin filament, J. Mol. Biol. 232 (1993) 334–341.
[57] M.P. Sheetz, D.B. Wayne, A.L. Pearlman, Extension of filopodia by motor-dependent actin assembly, Cell Motil. Cytoskeleton 22 (1992) 160–169.
[58] A. Tamada, S. Kawase, F. Murakami, H. Kamiguchi, Autonomous right-screw rotation of growth cone filopodia drives neurite turning, J. Cell Biol. 188 (2010) 429–441.
[59] R.P. Stevenson, D. Veltman, L.M. Machesky, Actin-bundling proteins in cancer progression at a glance, J. Cell Sci. 125 (2012) 1073–1079.
[60] Y. Hashimoto, M. Skacel, J.C. Adams, Roles of fascin in human carcinoma motility and signaling: prospects for a novel biomarker? Int. J. Biochem. Cell Biol. 37 (2005) 1787–1804.